ChemComm

ROYAL SOCIETY OF CHEMISTRY

COMMUNICATION

View Article Online
View Journal | View Issue

Cite this: *Chem. Commun.*, 2022, **58**, 7164

Received 21st December 2021,
Accepted 27th May 2022

DOI: 10.1039/d1cc07176a

rsc.li/chemcomm

Metallofullerene single-molecule magnet $Dy_2O@C_{2v}(5)$-C_{80} with a strong antiferromagnetic Dy···Dy coupling†

Georgios Velkos, ‡[a] Wei Yang,‡[ab] Yang-Rong Yao,[b] Svetlana M. Sudarkova,[ac] Fupin Liu,[a] Stanislav M. Avdoshenko,*[a] Ning Chen*[b] and Alexey A. Popov*[a]

Dysprosium-oxide clusterfullerene $Dy_2O@C_{2v}(5)$-C_{80} is a single-molecule magnet featuring antiferromagnetic superexchange Dy···Dy coupling *via* the μ_2-O^{2-} bridge, the strongest of its kind among {Dy_2} complexes with non-radical bridges.

The inner space of fullerenes allows stabilization of species comprising several metal and non-metal atoms. This turns endohedral metallofullerenes (EMFs) into a natural laboratory for the study of interactions in model systems, which can hardly be obtained by conventional chemical means.[1] For instance, short-distance bonding of endohedral lanthanide ions with non-metal ions, such as C^{4-} (ref. 2), N^{3-} (ref. 3), O^{2-} (ref. 4–6) or S^{2-} (ref. 7 and 8), leads to the strong magnetic axiality beneficial for single-molecule magnets (SMMs)[9] and earned EMFs a visible place among SMMs.[10] At the same time, confining two lanthanide ions inside a limited space of a carbon cage enhances their interaction and allows exploring the limits of exchange coupling between lanthanide magnetic moments. The first experimental studies of Dy-oxide clusterfullerenes $Dy_2O@C_{2n}$ revealed that their SMM performance and Dy···Dy interactions vary considerably with the fullerene cage.[4,5] Here we report on the isolation of a new Dy-oxide clusterfullerene, $Dy_2O@C_{80}$, and demonstrate that the SMM behaviour in this molecule is combined with the strongest antiferromagnetic Dy···Dy exchange interactions among Dy molecular magnets.

$Dy_2O@C_{80}$ was synthesized by an arc-discharge method and isolated by HPLC (see ESI†). Its molecular structure was determined by single-crystal X-ray diffraction of a co-crystal with Ni^{II} octaethylporphyrin (OEP).§ The fullerene cage coordinated by Ni(OEP) (Fig. 1a) is ordered and allows unambiguous assignment of the $C_{2v}(5)$ isomer, which is typical for C_{80}-based EMFs with 4-fold electron transfer and was first identified in $Sc_2C_2@C_{80}$,[11] and then in $Sc_2O@C_{80}$,[12] $Er_2C_2@C_{80}$,[13] and $Lu_2@C_{80}$.[14] Dy atoms are disordered over 10 sites. For the two sites with the highest occupancy of 0.38 and 0.36, the Dy–O–Dy angle is 154.2(3)° and the Dy–O distances are 1.999(5) and 2.005(5) Å. Since the disorder reduces the reliability of the structural parameters, DFT computations were performed to analyze possible positions and geometries of the Dy_2O cluster in $Dy_2O@C_{80}$.¶ Optimization of 120 uniformly distributed starting cluster orientations inside C_{80} resulted in only 4 unique conformers (see ESI†). The most stable one (Fig. 1b) coincides with the major Dy_2O cluster orientation in the X-ray structure. The DFT-optimized Dy–O–Dy angle is 145.2°, whereas the Dy–O bonds are 2.040 and 2.052 Å long.

The molecular structure of $Dy_2O@C_{2v}(5)$-C_{80} is further corroborated by spectroscopic studies. Excellent agreement between

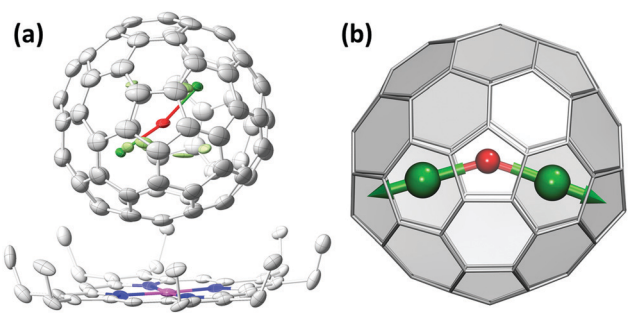

Fig. 1 (a) The $Dy_2O@C_{2v}(5)$-C_{80}·NiOEP moiety in the single crystal (30% probability ellipsoids); major Dy sites are shown in intense green, minor sites – pale green. (b) The lowest-energy DFT-computed conformer; green arrows show the directions of the Dy magnetic moments predicted by *ab initio* calculations.

[a] *Leibniz Institute for Solid State and Materials Research, Helmholtzstraße 20, 01069 Dresden, Germany. E-mail: s.avdoshenko@ifw-dresden.de, a.popov@ifw-dresden.de*
[b] *College of Chemistry, Chemical Engineering and Materials Science, Soochow University, Suzhou, Jiangsu, 215123, P. R. China. E-mail: chenning@suda.edu.cn*
[c] *Chemistry Department, Moscow State University, 119991 Moscow, Russia*

† Electronic supplementary information (ESI) available: Additional structural, computational and magnetic data. CCDC 2085187. For ESI and crystallographic data in CIF or other electronic format see DOI: https://doi.org/10.1039/d1cc07176a

‡ Equal contribution.

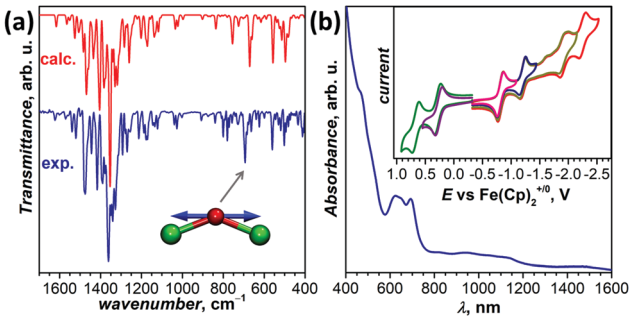

Fig. 2 (a) The experimental IR spectrum of $Dy_2O@C_{80}$ compared to the DFT-computed one for isostructural $Y_2O@C_{2v}(5)$-C_{80}; the arrow denotes the Dy–O stretching mode. (b) Vis-NIR absorption spectrum of $Dy_2O@C_{80}$ in CS_2; the inset shows the cyclic voltammogram of $Dy_2O@C_{80}$ in *o*-DCB/$TBAPF_6$.

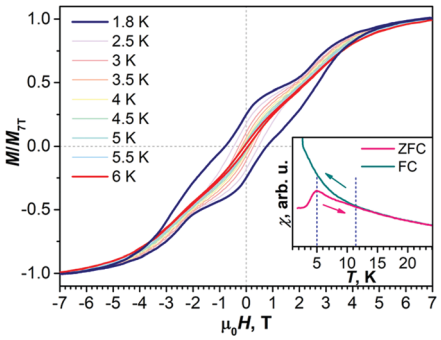

Fig. 3 Magnetic hysteresis of $Dy_2O@C_{80}$, at a sweep rate of 2.9 mT s^{-1}. Inset: FC and ZFC measurements; field 0.2 T, sweep rate 5 K min^{-1}.

experimental and calculated IR spectra supports the structural elucidation and enables the assignment of individual vibrational modes. The antisymmetric Dy–O stretching vibration is found at 693 cm^{-1}, within the range of 680–700 cm^{-1} found for this mode in other $Dy_2O@C_{2n}$ clusterfullerenes ($2n$ = 72, 74, and 82).[4,5] For comparison, Dy–O stretching vibrations in the matrix-isolated Dy–O species are found in the range of 600–850 cm^{-1}.[15]

The vis-NIR absorption spectrum of $Dy_2O@C_{80}$ with a strong feature at 600–700 nm resembles those of other EMFs with a $C_{2v}(5)$-C_{80} carbon cage.[11–13] $Dy_2O@C_{80}$ exhibits electrochemical activity with two oxidation and four reduction steps (Fig. 2b). The redox potentials (Table 1) and electrochemical gap of $Dy_2O@C_{80}$ are close to $Sc_2O@C_{80}$, but show a more pronounced difference to $Sc_2C_2@C_{80}$ and $Er_2C_2@C_{80}$, pointing to the involvement of the endohedral cluster in the redox processes.

The magnetic properties of powder $Dy_2O@C_{80}$ were studied by SQUID magnetometry. Temperature-dependent magnetization measurements for field-cooled (FC) and zero-field cooled (ZFC) samples show a peak in the ZFC curve at 5 K, but the bifurcation of the ZFC and FC curves happens at a higher temperature, near 11–12 K. Magnetic hysteresis of $Dy_2O@C_{80}$ is open up to 6 K (sweep rate of 2.9 mT s^{-1}). The shape of the hysteresis curves is quite remarkable. At 1.8 K, the coercivity is 0.65 T, but the hysteresis loop is open between –5 and 5 T. Besides, the curves measured during the field decrease show a pronounced inflection near 2 T (Fig. 3).

The magnetodynamics of $Dy_2O@C_{80}$ were evaluated by DC measurements of magnetization relaxation times, τ_M. The sample was magnetized at 7 T, and then the field was quickly swept to a required value, and then the decay of magnetization was recorded and fitted with a stretched exponential. Fig. 4a demonstrates that in the zero field, the temperature-dependence of τ_M follows the linear Arrhenius regime, switching to a levelling-off below 2.5 K. The temperature-independent relaxation is a characteristic of the quantum tunnelling of magnetization (QTM). Indeed, in a field of 0.1 T applied to suppress the QTM, τ_M grows with cooling without levelling-off and approaches $\sim 10^5$ s at 1.8 K. The fitting of the zero-field $\tau_M(T)$-dependence with a combination of Orbach and QTM relaxation processes, $\tau_M^{-1}(T) = \tau_0^{-1}\exp(-U^{eff}/T) + \tau_{QTM}^{-1}$, gives τ_{QTM} = 6600 ± 200 s and the barrier of U^{eff} = 26(1) K (18 cm^{-1}) with τ_0 = 31(2) ms. The U^{eff} value is much smaller than expected for the relaxation *via* excited ligand field states and is assigned to the exchange barrier, as discussed below.

The field-dependence of τ_M has a complex shape (Fig. 4b). First, near zero field, the relaxation times increase up to the maximum near 0.1 T. This regime is caused by a contribution of the QTM, which is gradually suppressed as the magnetic field increases. Then, τ_M starts to decrease, which is typical for the direct relaxation mechanism ($\tau_M^{-1} \sim H^nT$, n = 2–4). The gradual decay changes to a sharp dip when the field exceeds 1.5 T, with the shortest time recorded near 2 T. At the further field increase, τ_M grows again, and then switches to a decay above 2.5 T. The sharp negative peak in the field-dependence is an indication of an additional relaxation mechanism, which

Table 1 Redox potentials[a] of $Dy_2O@C_{2v}(5)$-C_{80} and other EMFs with a $C_{2v}(5)$-C_{80} cage

EMF	O-II	O-I	R-I	R-II	R-III	R-IV	Gap_{EC}
$Dy_2O@C_{80}$	0.67	0.27	−0.81	−1.19	−1.98	−2.24	1.08
$Sc_2O@C_{80}$[12]	0.56	0.24	−0.89	−1.48	−1.75	−1.96	1.13
$Sc_2C_2@C_{80}$[11]		0.41	−0.74	−1.33	−1.71	−2.04	1.15
$Er_2C_2@C_{80}$[13]		0.46	−0.80	−0.98	−1.77	−2.09	1.26

[a] Measured in $TBAPF_6$/*o*-dichlorobenzene and referred *versus* $Fe(Cp)_2^{+/0}$.

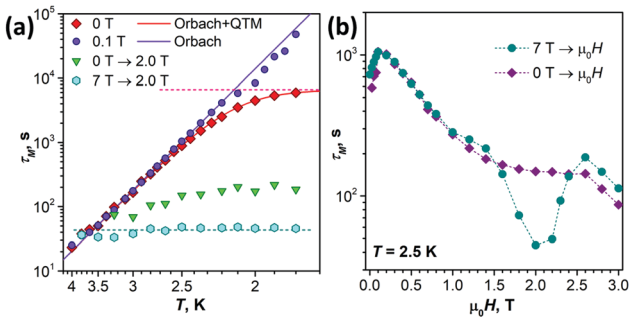

Fig. 4 Temperature-dependence (a) and magnetic field-dependence (b) of the magnetization relaxation time τ_M. The temperature-dependence was measured at 0 T, 0.1 T and 2.0 T. The temperature-dependence at 2 T and the field-dependence at 2.5 K were measured with the field ramped from 7 T and from 0 T, giving two sets of data.

steps in between 1.5 and 2.5 T and dominates the relaxation near 2 T. We suggest that this mechanism is the QTM at the anticrossing of the states with ferromagnetic (FM) and antiferromagnetic (AFM) alignment of Dy magnetic moments.[16] The QTM nature is further confirmed by the lack of temperature-dependence of τ_M measured at 2 T (Fig. 4a). Interestingly, when τ_M is measured not for the decay of magnetization after saturation at 7 T, but for the growth of magnetization after sweeping from zero field, the negative peak near 2 T is not observed (Fig. 4b).

The shape of the hysteresis curves points to the AFM coupling of Dy magnetic moments. The AFM coupling also follows from the shape of the χT curves (see ESI†). To obtain quantitative characteristics of the Dy···Dy coupling, we simulated magnetization curves using the Hamiltonian (1):

$$\hat{H}_{spin} = \hat{H}_{LF_1} + \hat{H}_{LF_2} - 2j_{12}\hat{J}_1 \cdot \hat{J}_2 + \hat{H}_{ZEE} \quad (1)$$

in which $\hat{H}_{LF_i}$ are the single-ion ligand-field terms and $\hat{H}_{ZEE}$ is the Zeeman term. The interaction of two Dy magnetic moments is described by the third term, in which j_{12} is the effective coupling constant, whereas $\hat{J}_i$ are the total angular momentum operators of Dy ions. The energy difference between the FM and AFM states in zero field is $\Delta E_{AFM\text{-}FM} = 225\, j_{12}\cos(\alpha)$, where α is the angle between two magnetic moments.

Single-ion magnetic properties were computed using MOLCAS at the CASSCF/SO-RASSI level.[17] The overall LF splitting for Dy ions exceeds 1400 cm^{-1}, and the energy difference between the ground state (essentially pure $m_J = \pm 15/2$) and the first excited doublet ($m_J = \pm 13/2$) is 410–420 cm^{-1} (see ESI†). The quantization axes are nearly coinciding with Dy–O bonds with a small deviation of 1–3° (Fig. 1b).

Hamiltonian (1) with *ab initio* ligand field parameters was then used to fit the experimental magnetization curves; j_{12} and α were set as free variables. The calculations were performed with the PHI code[18] and included powder averaging. A good agreement with experimental data was obtained for j_{12} of −0.12 cm^{-1} and α of 48.5°, yielding the $\Delta E_{AFM\text{-}FM}$ of −18.5 cm^{-1} (the dipolar and exchange contributions are 2.7 and −21.2 cm^{-1}, respectively). The $\Delta E_{AFM\text{-}FM}$ value of −18.5 cm^{-1} is unprecedentedly large for multinuclear Dy complexes with non-radical bridges. Before this work, the largest values in EMF-based {Dy_2} systems were 10.7 cm^{-1} in $Dy_2S@C_s$-C_{82}[7] and −12.9 cm^{-1} in $Dy_2O@C_{2v}$–C_{82},[5] whereas the largest $\Delta E_{AFM\text{-}FM}$ values in non-fullerene {Dy_2} complexes do not exceed 6–7 cm^{-1} (ref. 19).

The $\Delta E_{AFM\text{-}FM}$ energy from the fit is very close to the U^{eff} barrier determined from the temperature-dependence of τ_M, which confirms the interpretation of U^{eff} as the exchange barrier. Thus, the relaxation of magnetization in $Dy_2O@C_{80}$ at helium temperatures proceeds mainly *via* the flip of one of the Dy moments. A simultaneous flip of two Dy moments is a low-probability process, which is observed in zero field as the QTM with the long characteristic time of 6600 s.

The knowledge of the $\Delta E_{AFM\text{-}FM}$ and α values allows detailed analysis of the magnetic states and transitions between them. As magnetic moments of Dy ions (each 10 μ_B) in $Dy_2O@C_{80}$ are non-collinear, the moment of the AFM state is not zero but 8.2 μ_B, whereas the magnetic moment of the FM state is 18.2 μ_B (Fig. 5a). In a powder sample, molecules attain different orientations, and crossing of the FM and AFM levels depends on the angle between the magnetic field and a molecular frame. When the field direction is close to the direction of the magnetic moment of the AFM state, the latter remains the ground state in all fields. But for the majority of angles, one component of the FM pseudo-doublet ($|FM_+\rangle$) decreases its energy faster than the AFM component ($|AFM_+\rangle$), resulting in the switching of the ground state from $|AFM_+\rangle$ to $|FM_+\rangle$ in high magnetic fields (Fig. 5b).[20]

Fig. 5c shows the histograms for the fields, at which the $|FM_+\rangle$ energy level crosses $|AFM_-\rangle$ and $|AFM_+\rangle$ levels. The $|FM_+\rangle \leftrightarrow |AFM_+\rangle$ crossing is distributed with a considerable probability over the broad field range with the flat maximum near 2.6 T. On the contrary, the distribution of the $|FM_+\rangle \leftrightarrow |AFM_-\rangle$ crossing has a sharp peak near 2 T, exactly where the field-dependence of τ_M has a sharp minimum. In the large positive

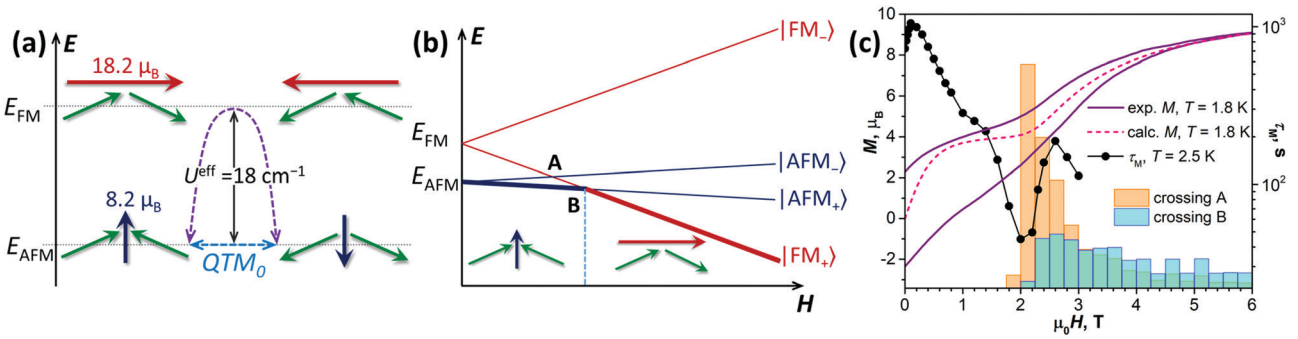

Fig. 5 (a) Two quasi-doublets with antiferromagnetic (AFM) and ferromagnetic (FM) alignments; green arrows denote magnetic moments of Dy ions, red and dark blue arrows are total moments of the $Dy_2O@C_{80}$ molecule in FM and AFM states; dashed arrows show the QTM in zero field and the Orbach mechanism *via* the FM state with the effective barrier U^{eff}. (b) Zeeman diagram for $Dy_2O@C_{80}$ for an arbitrary orientation of the molecule *versus* the magnetic field, where the total magnetic moment of the FM state is close to the parallel orientation; thick lines highlight the ground state in a given field range, and letters A and B mark $|FM_+\rangle \leftrightarrow |AFM_-\rangle$ and $|FM_+\rangle \leftrightarrow |AFM_+\rangle$ level crossing, respectively. (c) Histograms of the crossing events of type A and B in $Dy_2O@C_{80}$ computed for 10^5 uniformly distributed orientations of the magnetic field, overlaid with experimental hysteresis and calculated equilibrium magnetization curves at 1.8 K and the field-dependence of relaxation time at 2.5 K.

field, the majority of molecules are in the $|FM_+\rangle$ state. When the field is ramped down, the $|FM_+\rangle$ level first crosses the $|AFM_+\rangle$ level, and some molecules change their magnetic state to $|AFM_+\rangle$, but some still remain in the $|FM_+\rangle$ state and then undergo the second crossing, this time with the $|AFM_-\rangle$ level. At this crossing, the QTM appears to be more efficient, and besides that, the majority of crossing events are concentrated in a narrow field range, which altogether leads to a pronounced decrease of τ_M at the field, where the $|FM_+\rangle \leftrightarrow |AFM_-\rangle$ crossing distribution has a maximum. The $|FM_+\rangle \leftrightarrow |AFM_+\rangle$ crossing does not produce an analogous dip of τ_M because the number of events is smaller and they are distributed more uniformly in a broader field range.

To conclude, we obtained clusterfullerene $Dy_2O@C_{2v}(5)$-C_{80} and showed that it behaves as a single-molecule magnet. The molecule features the strongest exchange coupling of Dy magnetic moments among $\{Dy_2\}$ molecular magnets.

The authors thank beamline BL17B of the Shanghai Synchrotron Radiation Facility for single crystal measurements and acknowledge financial support by Deutsche Forschungsgemeinschaft (Grants PO 1602/7-1, LI 3055/3-1, and AV 169/3-1) and the National Science Foundation of China (NSFC 91961109 to N. C.).

Conflicts of interest

There are no conflicts to declare.

Notes and references

§ $Dy_2O@C_{2v}(5)$-C_{80}·Ni(OEP) crystals were measured at 100 K using the synchrotron radiation (0.82653 Å) at the Shanghai Synchrotron Radiation Facility. The structure was solved by direct methods[21] using the SHELXL2015 crystallographic software package.[22] The disordered solvent molecules are masked with SQUEEZE code.[23] The crystal data are presented in the ESI. The data can be obtained free of charge from the Cambridge Crystallographic Data Centre with CCDC No. 2085187.
¶ DFT calculations were performed first at the PBE/TZ2P level for $Y_2O@C_{80}$ (Priroda[24]); the structures were then re-optimized with Dy at the PBE-D/PAW level with 4f-in-core potentials (VASP 5.0[25]).

1 A. A. Popov, S. Yang and L. Dunsch, *Chem. Rev.*, 2013, **113**, 5989; S. Yang, T. Wei and F. Jin, *Chem. Soc. Rev.*, 2017, **46**, 5005; X. Lu, W. Shen and S. Hu, *Chem. – Eur. J.*, 2020, **26**, 5748; L. Feng, Y. Hao, A. Liu and Z. Slanina, *Acc. Chem. Res.*, 2019, **52**, 1802; W. Cai, C.-H. Chen, N. Chen and L. Echegoyen, *Acc. Chem. Res.*, 2019, **52**, 1824.
2 R. Westerström, V. Dubrovin, K. Junghans, C. Schlesier, B. Büchner, S. M. Avdoshenko, A. A. Popov, A. Kostanyan, J. Dreiser and T. Greber, *Phys. Rev. B*, 2021, **104**, 224401; K. Junghans, C. Schlesier, A. Kostanyan, N. A. Samoylova, Q. Deng, M. Rosenkranz, S. Schiemenz, R. Westerström, T. Greber, B. Büchner and A. A. Popov, *Angew. Chem., Int. Ed.*, 2015, **54**, 13411; A. Brandenburg, D. S. Krylov, A. Beger, A. U.-B. Wolter, B. Büchner and A. A. Popov, *Chem. Commun.*, 2018, **54**, 10683.
3 L. Spree, C. Schlesier, A. Kostanyan, R. Westerström, T. Greber, B. Büchner, S. Avdoshenko and A. A. Popov, *Chem. – Eur. J.*, 2020, **26**, 2436; A. Kostanyan, R. Westerström, D. Kunhardt, B. Büchner, A. A. Popov and T. Greber, *Phys. Rev. B*, 2020, **101**, 134429; R. Westerström, J. Dreiser, C. Piamonteze, M. Muntwiler, S. Weyeneth, K. Krämer, S.-X. Liu, S. Decurtins, A. Popov, S. Yang, L. Dunsch and T. Greber, *Phys. Rev. B: Condens. Matter Mater. Phys.*, 2014, **89**, 060406; R. Westerström, J. Dreiser, C. Piamonteze, M. Muntwiler, S. Weyeneth, H. Brune, S. Rusponi, F. Nolting, A. Popov, S. Yang, L. Dunsch and T. Greber, *J. Am. Chem. Soc.*, 2012, **134**, 9840; M. Nie, J. Xiong, C. Zhao, H. Meng, K. Zhang, Y. Han, J. Li, B. Wang, L. Feng, C. Wang and T. Wang, *Nano Res.*, 2019, **12**, 1727; D. S. Krylov, F. Liu, S. M. Avdoshenko, L. Spree, B. Weise, A. Waske, A. U.-B. Wolter, B. Büchner and A. A. Popov, *Chem. Commun.*, 2017, **53**, 7901.
4 G. Velkos, W. Yang, Y.-R. Yao, S. M. Sudarkova, X. Liu, B. Büchner, S. M. Avdoshenko, N. Chen and A. A. Popov, *Chem. Sci.*, 2020, **11**, 4766.
5 W. Yang, G. Velkos, F. Liu, S. M. Sudarkova, Y. Wang, J. Zhuang, H. Zhang, X. Li, X. Zhang, B. Büchner, S. M. Avdoshenko, A. A. Popov and N. Chen, *Adv. Sci.*, 2019, **6**, 1901352.
6 M. K. Singh and G. Rajaraman, *Chem. Commun.*, 2016, **52**, 14047.
7 D. Krylov, G. Velkos, C.-H. Chen, B. Büchner, A. Kostanyan, T. Greber, S. Avdoshenko and A. A. Popov, *Inorg. Chem. Front.*, 2020, **7**, 3521.
8 C.-H. Chen, D. S. Krylov, S. M. Avdoshenko, F. Liu, L. Spree, R. Yadav, A. Alvertis, L. Hozoi, K. Nenkov, A. Kostanyan, T. Greber, A. U.-B. Wolter and A. A. Popov, *Chem. Sci.*, 2017, **8**, 6451; W. Cai, J. D. Bocarsly, A. Gomez, R. J. Letona Lee, A. Metta-Magaña, R. Seshadri and L. Echegoyen, *Chem. Sci.*, 2020, **11**, 13129.
9 D. Shao and X.-Y. Wang, *Chin. J. Chem.*, 2020, **38**, 1005; K. L.-M. Harriman, D. Errulat and M. Murugesu, *Trends Chem.*, 2019, **1**, 425; J.-L. Liu, Y.-C. Chen and M.-L. Tong, *Chem. Soc. Rev.*, 2018, **47**, 2431.
10 L. Spree and A. A. Popov, *Dalton Trans.*, 2019, **48**, 2861; F. Liu, L. Spree, D. S. Krylov, G. Velkos, S. M. Avdoshenko and A. A. Popov, *Acc. Chem. Res.*, 2019, **52**, 2981; W. Li, C.-R. Wang and T. Wang, *Chem. Commun.*, 2021, **57**, 10317.
11 H. Kurihara, X. Lu, Y. Iiduka, N. Mizorogi, Z. Slanina, T. Tsuchiya, T. Akasaka and S. Nagase, *J. Am. Chem. Soc.*, 2011, **133**, 2382.
12 Q. Tang, L. Abella, Y. Hao, X. Li, Y. Wan, A. Rodríguez-Fortea, J. M. Poblet, L. Feng and N. Chen, *Inorg. Chem.*, 2015, **54**, 9845.
13 S. Hu, P. Zhao, W. Shen, M. Ehara, Y. Xie, T. Akasaka and X. Lu, *Inorg. Chem.*, 2020, **59**, 1940.
14 W. Shen, L. Bao, S. Hu, L. Yang, P. Jin, Y. Xie, T. Akasaka and X. Lu, *Chem. Sci.*, 2019, **10**, 829.
15 S. P. Willson and L. Andrews, *J. Phys. Chem. A*, 1999, **103**, 6972.
16 F. Pointillart, Y. Le Gal, S. Golhen, O. Cador and L. Ouahab, *Chem. – Eur. J.*, 2011, **17**, 10397.
17 F. Aquilante, J. Autschbach, A. Baiardi, S. Battaglia, V. A. Borin, L. F. Chibotaru, I. Conti, L. D. Vico, M. Delcey, I. F. Galván, N. Ferré, L. Freitag, M. Garavelli, X. Gong, S. Knecht, E. D. Larsson, R. Lindh, M. Lundberg, P. Å. Malmqvist, A. Nenov, J. Norell, M. Odelius, M. Olivucci, T. B. Pedersen, L. Pedraza-González, Q. M. Phung, K. Pierloot, M. Reiher, I. Schapiro, J. Segarra-Martí, F. Segatta, L. Seijo, S. Sen, D.-C. Sergentu, C. J. Stein, L. Ungur, M. Vacher, A. Valentini and V. Veryazov, *J. Chem. Phys.*, 2020, **152**, 214117; L. F. Chibotaru and L. Ungur, *J. Chem. Phys.*, 2012, **137**, 064112.
18 N. F. Chilton, R. P. Anderson, L. D. Turner, A. Soncini and K. S. Murray, *J. Comput. Chem.*, 2013, **34**, 1164.
19 W. Zhang, S.-M. Xu, Z.-X. Zhu, J. Ru, Y.-Q. Zhang and M.-X. Yao, *New J. Chem.*, 2020, **44**, 2083; X.-Q. Ji, F. Ma, J. Xiong, J. Yang, H.-L. Sun, Y.-Q. Zhang and S. Gao, *Inorg. Chem. Front.*, 2019, **6**, 786; P. Zhang, F. Benner, N. F. Chilton and S. Demir, *Chem*, 2022, **8**, 717; J. Wang, Q.-W. Li, S.-G. Wu, Y.-C. Chen, R.-C. Wan, G.-Z. Huang, Y. Liu, J.-L. Liu, D. Reta, M. J. Giansiracusa, Z.-X. Wang, N. F. Chilton and M.-L. Tong, *Angew. Chem., Int. Ed.*, 2021, **60**, 5299.
20 X. Yi, K. Bernot, F. Pointillart, G. Poneti, G. Calvez, C. Daiguebonne, O. Guillou and R. Sessoli, *Chem. – Eur. J.*, 2012, **18**, 11379.
21 O. V. Dolomanov, L. J. Bourhis, R. J. Gildea, J. A.-K. Howard and H. Puschmann, *J. Appl. Crystallogr.*, 2009, **42**, 339.
22 G. Sheldrick, *Acta Crystallogr., Sect. C: Struct. Chem.*, 2015, **71**, 3.
23 A. Spek, *Acta Crystallogr., Sect. C: Struct. Chem.*, 2015, **71**, 9.
24 D. N. Laikov and Y. A. Ustynuk, *Russ. Chem. Bull.*, 2005, **54**, 820.
25 J. Hafner, *J. Comput. Chem.*, 2008, **29**, 2044; G. Kresse and J. Hafner, *Phys. Rev. B: Condens. Matter Mater. Phys.*, 1993, **47**, 558; G. Kresse and D. Joubert, *Phys. Rev. B: Condens. Matter Mater. Phys.*, 1999, **59**, 1758; J. P. Perdew, K. Burke and M. Ernzerhof, *Phys. Rev. Lett.*, 1996, **77**, 3865; S. Grimme, *Wiley Interdiscip. Rev.: Comput. Mol. Sci.*, 2011, **1**, 211.